Hindawi
International Journal of Optics
Volume 2019, Article ID 8782567, 14 pages
https://doi.org/10.1155/2019/8782567

Research Article

Optical Identification of *Plasmodium falciparum* Malarial Byproduct for Parasite Density Estimation

Jerry Opoku-Ansah,[1,2] **Moses Jojo Eghan**,[1,2] **Benjamin Anderson**,[1,2] **Johnson Nyarko Boampong**,[3] **Raymond Edziah**,[1,2] **Peter Osei-Wusu Adueming**,[1,2] **and Charles Lloyd Yeboah Amuah**[1,2]

[1]*Laser and Fibre Optics Centre, School of Physical Sciences, College of Agriculture and Natural Sciences, University of Cape Coast, Cape Coast, Ghana*
[2]*Department of Physics, School of Physical Sciences, College of Agriculture and Natural Sciences, University of Cape Coast, Cape Coast, Ghana*
[3]*Department of Biomedical Science, School of Allied Health Sciences, College of Health and Allied Sciences, University of Cape Coast, Cape Coast, Ghana*

Correspondence should be addressed to Jerry Opoku-Ansah; jopoku-ansah@ucc.edu.gh

Received 18 April 2019; Accepted 14 October 2019; Published 11 November 2019

Academic Editor: Qin Zhou

Plasmodium falciparum (*P. falciparum*) malarial degree of infection, termed as parasite density (PD), estimation is vital for point-of-care diagnosis and treatment of the disease. In this work, we present application of optical techniques: optical absorption and multispectral imaging for *P. falciparum* malarial byproduct (hemozoin) detection in human-infected blood samples to estimate PD. The blood samples were collected from volunteers who were tested positive for *P. falciparum* infections (*i*-blood), and after treatment, another set of blood samples (*u*-blood) were also taken. The *i*-blood samples were grouped based on PD (+, ++, +++, and ++++). Optical densities (ODs) of *u*-blood samples and *i*-blood samples at blood absorption bands of 405 nm, 541 nm, and 577 nm showed different optical absorption characteristics. Empirical computation of ratio of the ODs for the blood absorption bands revealed reduction in the ODs with increasing PD. Multispectral images containing uninfected red blood cells (*u*-RBCs) and *P. falciparum*-infected red blood cells (*i*-RBCs) on unstained blood smear slides exhibited spectrally determined decrease in both reflected and scattered pixel intensities and increase in transmitted pixel intensities with increasing PD. We further propose a linear classification model based on Fisher's approach using reflected, scattered, and transmitted pixel intensities for easy and inexpensive estimation of PD as an alternative to manual estimation of PD, currently, the widely used technique. Application of the optical techniques and the proposed linear classification model are therefore recommended for improved malaria diagnosis and therapy.

1. Introduction

Plasmodium falciparum (*P. falciparum*) malarial parasite density (PD) estimation provides salient information on the severity of the disease and treatment response. During intraerythrocytic development stage, these parasites feed on hemoglobin (Hb) of their hosts red blood cells (RBCs) [1, 2], resulting in hemozoin production as a byproduct [3–6]. Research has shown that the production of the hemozoin correlates linearly with PD in the blood [7, 8]. The Hb has been found to absorb light strongly around 405 nm, referred to as Soret band (*S*-band). Other absorption bands are found around 541 nm, beta band (β-band), and 577 nm, alpha band (α-band) [9–11].

In clinical settings, the level of PD is helpful as one of the criteria used to monitor the effect of antimalarial treatment [12]. When the PD of a *P. falciparum*-infected patient is known, the right antimalarial drug dosage can be prescribed

for treatment, and this will help prevent underdose or overdose and their associated toxicity [13, 14]. Hence, instant PD estimation could provide a quick solution for precise prescription of antimalarial drugs. Even though widely used manual examination technique for PD estimation exists for *P. falciparum* malarial [15–18], it uses Giemsa-stained thick or thin blood smear slides under light microscope. This technique is time-consuming, costly, destructive, and sometimes results in experts giving subjective results [19–24]. Therefore, there is the need for a fast, objective, nondestructive, and relatively less expensive technique to address this problem. Optical techniques (OTs) are considered favorable candidates to use because they have already found many applications in supporting medical treatment.

Optical techniques, in principle, are versatile, relatively fast and less expensive, nondestructive, and valuable being used for the diagnosis of diseases [25–28]. They are said to be the only techniques that can provide cellular or molecular level information about samples, with almost single molecule sensitivity, allowing probing of cellular structure and dynamics for understanding the mechanisms of physiological regulation [29, 30]. OTs such as optical absorption (OA) and multispectral imaging (MSI) are being applied for hemozoin detection, providing comparable results in malaria diagnosis [24, 31–33]. The OA spectra and the influence of refractive index (RI) are more likely to differ when a higher spectral resolution is accessible. Hence, increasing the number of acquisition channels ensures easier identification of objects.

Multispectral imaging, which has many applications including microscopy [34], is the act of capturing images at more than one spectral band and extracting physical as well as chemical properties information out of the images and is dependent on excitation light source used during acquisition [35]. When microscopy of a sample is done in transmission mode, contrast occurs partially from differences in absorption properties of different parts of the sample and partly from spatial gradients in the RI. A measure of a pixel intensity (I) extracted from an image acquired at a spectral band is given as

$$I = \int_0^\infty E_{\mathrm{sp}}(\lambda) T(\lambda) S_{\mathrm{B}}(\lambda) \mathrm{d}\lambda, \quad (1)$$

where E_{sp} is the emission spectrum of illumination, T is the ratio of transmitted intensity to incident intensity, S_{B} is the spectral band of the imaging system, and λ is the wavelength of the illumination light source. Equation (1) shows that a result is achieved when there is a convergence among the emission spectrum of illumination, the spectral band of the imaging system, and the wavelength of the illumination light source.

Malarial studies involving OA include interpreting ultraviolet-visible spectra of malarial parasite *P. falciparum* [36], optical properties of malaria parasites in infected RBCs (*i*-RBCs) [24, 37], birefringence quantitative monitoring of uninfected RBCs (*u*-RBCs) and *i*-RBCs [38], magneto-optic route toward in vivo diagnosis of malaria [39], and miniaturized optical diagnostic method by spectrophotometry for hemozoin quantification [40]. MSI studies comprise wavelength markers for identifying ring and trophozoite stages of *P. falciparum* parasites [41], application of principal component analysis to multimodal optical image analysis for malaria diagnostics [42], multimode light-emitting diode microscopy for malaria diagnostics [43], and rapid malaria diagnosis by light microscope with interference filter [44]. To the best of our knowledge, OA and MSI techniques have not been combined for PD estimation from *P. falciparum*–infected blood samples of human.

In the present work, we employ OA and MSI techniques for hemozoin identification in *P. falciparum*-infected human blood samples for PD estimation. These techniques are being introduced to complement the laser-induced autofluorescence technique that has been developed by the group [45].

2. Experimental Methods and Procedure

2.1. Blood Sample Preparation. Five millilitres (5 ml) each of blood samples were collected from 80 positively tested malaria parasites-infected volunteers. The same amount of blood samples was collected from the same volunteers after antimalarial treatment and those tested negative (uninfected), totaling 160 blood samples. The infected blood samples were grouped, by an expert, into four categories (+, ++, +++, and ++++) based on the level of infection, PD. Three millilitres (3 ml) each of the blood samples, both infected (*i*-blood) and uninfected (*u*-blood) samples, were used in preparing 8 thin blood smear slides, 3 stained and 5 unstained, following protocol described by Boampong et al. [46], for microscopy imaging. The stained sets were used as training slides and unstained set as test slides. The volunteers were informed about the study, and appropriate consents were obtained. The blood samples and volunteer's data collection procedures were approved by the Ghana Health Service Ethical Review Committee (GHS-ERC-09/05/14). Finger prick technique was used to collect the blood sample from all the volunteers. The volunteers were 40% males and 60% females aging between 1 and 89 years with a mean age of 16 years.

2.2. Optical Absorption Measurements. For quantitative determination of Hb concentration in *u*-blood and *i*-blood samples, Drabkin's solution was prepared from distilled water (1 L), potassium dihydrogen phosphate (140 mg), potassium ferricyanide (200 mg), potassium cyanide (50 mg), and nonionic detergent (1 ml). Referenced optical densities (ODs) were measured with UV-VIS spectrophotometer (Shimadzu UVmini-1240, Japan), at 405 nm (S-band), 541 nm (β-band), and 577 nm (α-band) using 2.5 ml of the Drabkin's solution.

Three ODs of a mixture of twelve microliters (12 μl) of *u*-blood and 2.5 ml of the Drabkin's solution were measured for each band using the same spectrophotometer. The measurement procedures were repeated for all the *i*-blood samples. ODs for the blood samples were calculated by

subtracting the referenced ODs from the ODs obtained from a mixture of the Drabkin's solution and the blood samples.

2.3. Multispectral Image Acquisitions. Using a multispectral light-emitting diode imaging (MSLEDI) microscope, described somewhere else [47], multispectral images of *i*-blood smears and *u*-blood smears were acquired in reflection, scattering, and transmission modes. For each slide of blood smear and for each mode, 13 images were acquired using 13 different LED sources. The image acquisitions were done without changing the sample position for an accurate prediction on the optical characteristics of each pixel for all the three modes. The images were then separated into training and test sets, for both *i*-blood and *u*-blood, for analysis. All analyses in this work were done using MATrix LABoratory (Matlab) (R2014a Matlab 7.10.0, MathWorks Inc., USA).

2.4. Data Processing

2.4.1. Ratio of Optical Density Calculation. The referenced ODs data, as well as the ODs data comprising a mixture of the Drabkin's solution and the blood samples, measured at the *S*-band, the β-band, and the α-band were imported into Matlab platform. In the Matlab platform, ODs for each *u*-blood and *i*-blood samples were calculated using the following equation:

$$\mathrm{OD}_{(\mathrm{sample})} = \mathrm{OD}_{(\mathrm{Drabkin's+sample})} - \mathrm{OD}_{(\mathrm{Drabkin's})}. \quad (2)$$

The *u*-blood samples are composed of Hb, and their spectra are dominated by the spectral fingerprint of the Hb, which is strongly characterized by the *S*-band, the β-band, and the α-band [48]. Ratios of ODs at the β-band to the α-band and as a product of the *S*-band were, respectively, calculated using an empirical relation:

$$\mathrm{OD}_{(\beta/\alpha)(S)} = \left[\left(\frac{\mathrm{OD}_{\beta-\mathrm{band}}}{\mathrm{OD}_{\alpha-\mathrm{band}}}\right)\left(\mathrm{OD}_{S-\mathrm{band}}\right)\right] + k, \quad (3)$$

where k is a constant ODs factor. Equation (3) is a modified version of the model presented by Antonini and Brunori [49].

2.4.2. Linear Discriminant Analysis. Linear discriminant analysis (LDA) is a commonly used multivariate technique for data classification. For a data set containing two groups, say *u*-RBCs and *i*-RBCs, the LDA can be used for classification using the following relation [50]:

$$\mathrm{LDA} = (Dv)' x \left(\overline{\mathrm{PC}_{u-\mathrm{RBCs}}} - \overline{\mathrm{PC}_{i-\mathrm{RBCs}}}\right)' (\mathrm{Cov})^{-1} \mathrm{PC}_x, \quad (4)$$

where Dv is the discriminant vector, $\mathrm{PC}_{u-\mathrm{RBCs}}$ and $\mathrm{PC}_{i-\mathrm{RBCs}}$ are the average values of the principal components (PCs) from the two groups, Cov is the common covariance matrix of the two groups, and PC_x is the average PC values of the RBCs to be classified. A new observation PC_{xo} can be assigned to *u*-RBCs, if

$$\mathrm{LDA}_{(0)} = \left(\overline{\mathrm{PC}_{u-\mathrm{RBCs}}} - \overline{\mathrm{PC}_{i-\mathrm{RBCs}}}\right)' (\mathrm{Cov})^{-1} \mathrm{PC}_{xo} \geq \mathrm{mp}, \quad (5)$$

where

$$\mathrm{mp} = \frac{1}{2}\left(\overline{\mathrm{PC}_{u-\mathrm{RBCs}}} - \overline{\mathrm{PC}_{i-\mathrm{RBCs}}}\right)' (\mathrm{Cov})^{-1} \left(\overline{\mathrm{PC}_{u-\mathrm{RBCs}}} + \overline{\mathrm{PC}_{i-\mathrm{RBCs}}}\right). \quad (6)$$

is the midpoint between the two groups' averages, else PC_{xo} is assigned to i-RBCs if

$$\mathrm{LDA}_{(o)} < \mathrm{mp}. \quad (7)$$

Fisher's linear discriminant analysis (FLDA) was performed using the pixel intensities data extracted from the images captured at two discriminating spectral bands (2-DSBs): 435 nm and 660 nm. The FLDA of the pixel intensities data follows a procedure described by Adueming et al. [51]. Allocation rule obtained from the FLDA function for the pixel intensities data of the *u*-RBCs and the *i*-RBCs) is given as

$$\mathrm{LDA}_{(o)} = K_1 \mathrm{PC}_1 + K_2 \mathrm{PC}_2 + K_3 \mathrm{PC}_3, \quad (8)$$

where PC_1, PC_2, and PC_3 represent first, second, and third PCs, respectively, with K_1, K_2, and K_3 being the coefficient of the PCs. Thus, if $\mathrm{PC}_{xo} \geq \mathrm{mp}$, then the pixel intensities belong to the *u*-RBC, else they are the *i*-RBCs.

3. Results

3.1. Optical Absorption. The mean ODs of the *u*-blood and the *i*-blood samples for *S*-band, β-band, and α-band, after one-way ANOVA are shown in Table 1. The mean ODs and their respective deviations from the mean are presented in the third, fourth, and fifth columns, and the eighth row shows the p values. The p values indicate the differences between ODs of the *u*-blood and *i*-blood samples. Variations can be observed in the ODs for the *i*-blood samples in relation to the *u*-blood samples at the *S*-band, the β-band, and the α-band. Except the α-band, the two other bands (*S*- and β-bands) show high ODs for the *u*-blood samples. In the case of the *i*-blood, the ODs of the *S*-band reduces with increasing PD, whereas that of the α-band increases with increasing PD. But the same trend cannot be said of the β-band. The β-band shows increasing ODs with increasing PDs from (+) to (+++) and reduction in ODs for PD of (++++).

The ratio of the β-band to α-band ODs for the *u*-blood samples reduces by about 2.3% as compared with the literature value of 0.9200% [49]. The ODs were slightly high in PD of (+) and reduced in (++), (+++), and (++++). A graphical representation of the PD empirical model, equation (3), is presented in Figure 1.

Patterns of distribution, as indicated by the error bars in Figure 1, show the highest ODs ratio for the *u*-RBCs and reduction in the ratios of ODs with increasing PD in the *i*-RBCs. This observation suggests that adding the *S*-band as a product of the ratio of the β-to α-bands ODs would give better information because the *S*-band is a strong Hb absorption band. Hence, one could easily make predictions for

Table 1: Optical densities of uninfected and *Plasmodium falciparum*-infected blood samples of different parasite density at *S*-band, β-band, and α-band.

Blood samples		Mean optical densities (ODs) (a.u.)			
		S-band	α-band	β-band	$OD_{(\beta/\alpha)(S)}$
u-blood		$1.07^{a} \pm 0.01$	$0.10^{a} \pm 0.05$	$0.09^{a} \pm 0.01$	0.96 ± 0.01
i-blood (PD)	(+)	$1.04^{a} \pm 0.01$	$0.08^{b} \pm 0.01$	$0.05^{b} \pm 0.02$	0.65 ± 0.01
	(++)	$0.99^{b} \pm 0.06$	$0.10^{c} \pm 0.01$	$0.06^{c} \pm 0.01$	0.59 ± 0.03
	(+++)	$0.71^{c} \pm 0.03$	$0.15^{d} \pm 0.03$	$0.08^{a} \pm 0.01$	0.38 ± 0.01
	(++++)	$0.64^{d} \pm 0.06$	$0.17^{e} \pm 0.01$	$0.07^{a} \pm 0.02$	0.26 ± 0.01
p value		<0.0001	<0.0001	<0.0001	<0.0001

Comparing *u*-blood samples to *i*-blood samples, mean ODs with different superscript along the columns are significantly different.

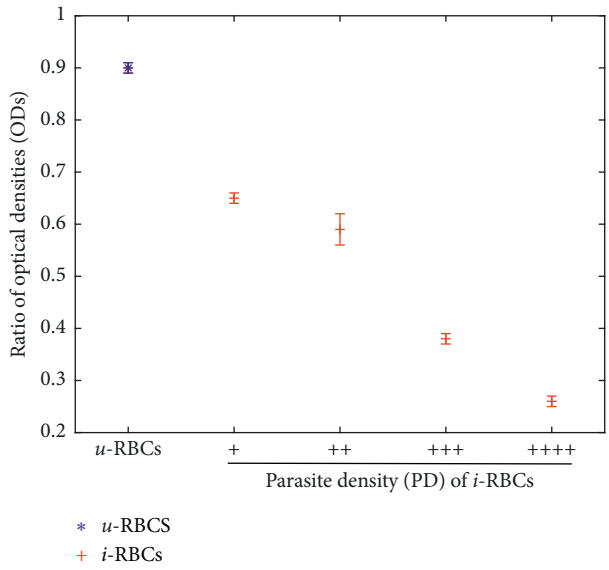

Figure 1: Optical densities ratio measured at blood absorption bands for uninfected RBCs (*u*-RBCs) and *Plasmodium falciparum*-infected RBCs (*i*-RBCs) of different parasite density (PD) (+), (++), (+++), and (++++).

PD estimations in human blood when the *S*-band is considered.

3.2. Multispectral Images

3.2.1. Color Representation of Multispectral Images. Figure 2 shows pseudocolor images of *u*-RBCs and *i*-RBCs from 660 nm (R), 525 nm (G), and 435 nm (B), as was done by Merdasa et al. [43]. These spectral bands have been identified as markers for discriminating *i*-RBCs and *u*-RBCs using the MSI technique [41]. The RGB images (Figure 2), if color printed, show features of RBCs as they appear under an optical microscope. Figure 2 also shows the same region of the blood smear slides under the MSLEDI microscope in all the three modes.

Figures 2(a)–2(c) show differences in the color images of the RBCs in all the three modes. In Figure 2(a), some RBCs appear dark in the center, suggesting a decrease in reflection in the RBCs. This observation seems to differ among other RBCs. Some RBCs also appear white in the center, indicating high reflection. In Figure 2(b), it can be observed that some RBCs seem to have an internal structure. RBCs with internal structure are more scattered, whereas those without the structure appear to have unfilled centers. Figure 2(c) shows the predicted RBCs color (red color), but there is a clear distinction between the RBCs. Some RBCs appear slightly brownish indicating low transmission whereas others appear redder with high transmission.

3.2.2. Feature Extraction of Hemozoin Properties. Pixel intensities of images containing the *u*-RBCs and the *i*-RBCs for the 13 spectral bands were extracted. Figures 3–5 show three-dimensional (3D) plots of the pixel intensities, I (a.u) and radii, r (μm) of the *u*-RBCs and the *i*-RBCs with different PD against spectral range, λ (nm) for reflection, scattering, and transmission modes, respectively. The 3D surf plots in Figures 3–5 show, to some extent, spectral variations in pixel intensities extracted from the *u*-RBCs and the *i*-RBCs in all the modes. The existence of hemozoin, or the decrease in Hb concentration, appears in all the three acquisition modes, suggesting the prevalence of infection. Figure 3(a) shows the highest reflected intensity and the typical RBCs color in the red spectral band. In Figures 3(b)–3(e), there is reduction in reflected intensity as the PD increases. The RBCs color almost disappears even with (+) PD and the blue color increases with increasing PD. These observations are as a result of the fact that in the red spectral band, the *u*-RBCs show high reflection of red light and the presence of hemozoin and/or increase in PD in the *i*-RBCs shifts RBCs light reflection to lower wavelength (blue region) in the electromagnetic spectrum. Figures 4(a)–4(e) shows scattering at the edges for both the *u*-RBCs and the *i*-RBCs within the red spectral band. The *u*-RBCs lack internal structures and therefore could not scatter red light at the center. Figures 5(a)–5(e) shows a clear optical characteristic distinction between the *u*-RBCs and the *i*-RBCs. Figures 5(a)–5(e) shows transmission of red light through the center of the *u*-RBCs and *i*-RBCs. Due to the presence of hemozoin and a reduction in Hb, which makes the *i*-RBCs less dense, there is an increase in the pixel intensities and a decrease in RBCs color as the PD increased (Figures 5(b)–5(e)).

The pixel intensities data extracted from the images at the 2-DSBs are in the coordinates of the first two Fisher's discriminants, and the results are presented in Figures 6–9. Figures 6(a)–6(d) show scatter plots of the first two Fisher's

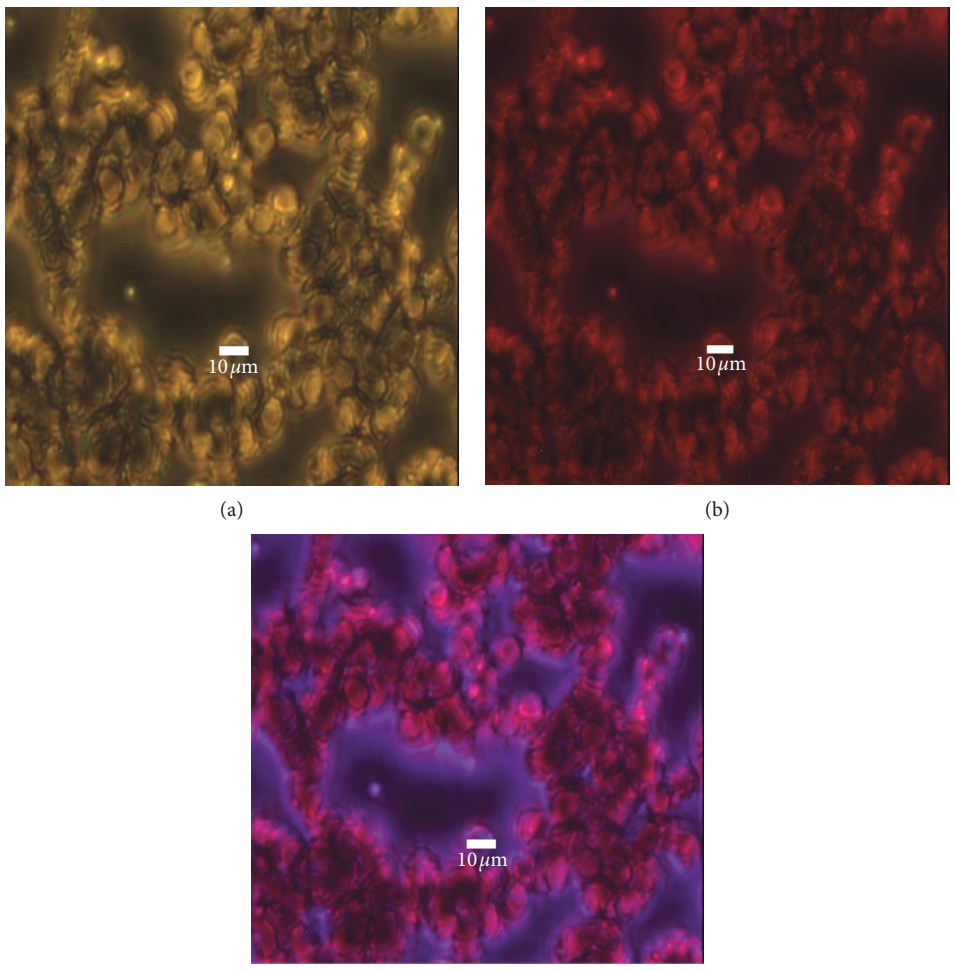

FIGURE 2: Pseudocolor (a–c) red, green, and blue (RGB) representation of images acquired from three modes with the aid of a multispectral light-emitting *diode* imaging microscope. Each image consists of combined images of 660 nm (R), 525 nm (G), and 435 nm (B). (a) Reflection mode shows shades of white in most of RBCs, indicating a reduction in reflection in some RBCs with dark spots in the center. (b) Scattering mode depicts dimmer or less scattering for some RBCs. (c) Transmission mode shows some RBCs absorbing more light than others in the center of the RBCs, hence appearing as dark spots.

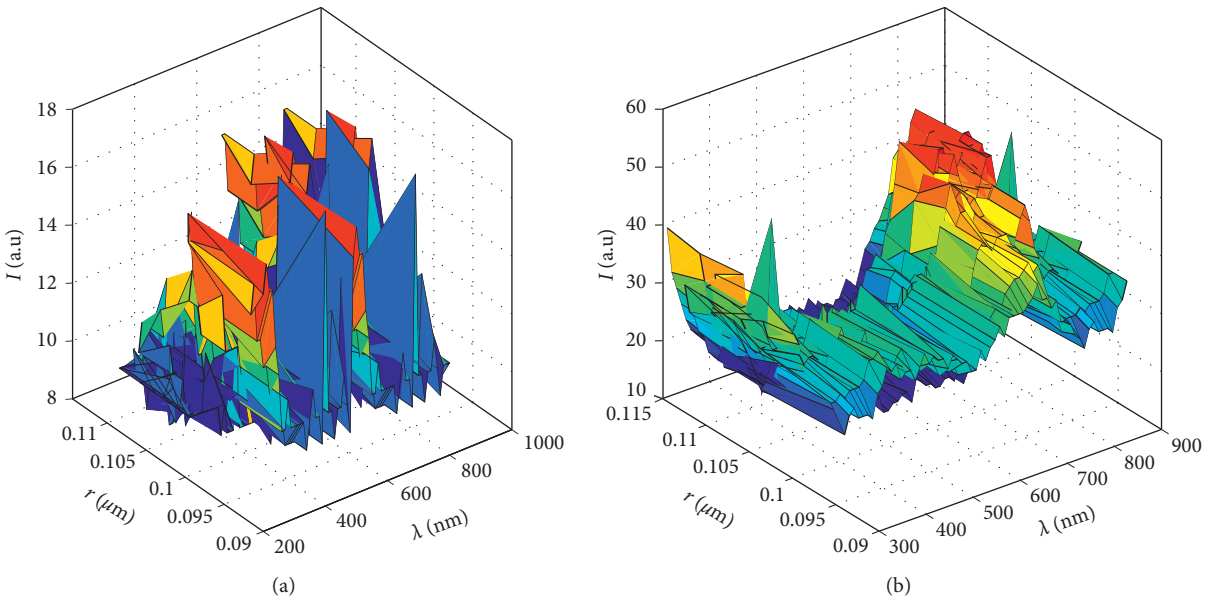

FIGURE 3: Continued.

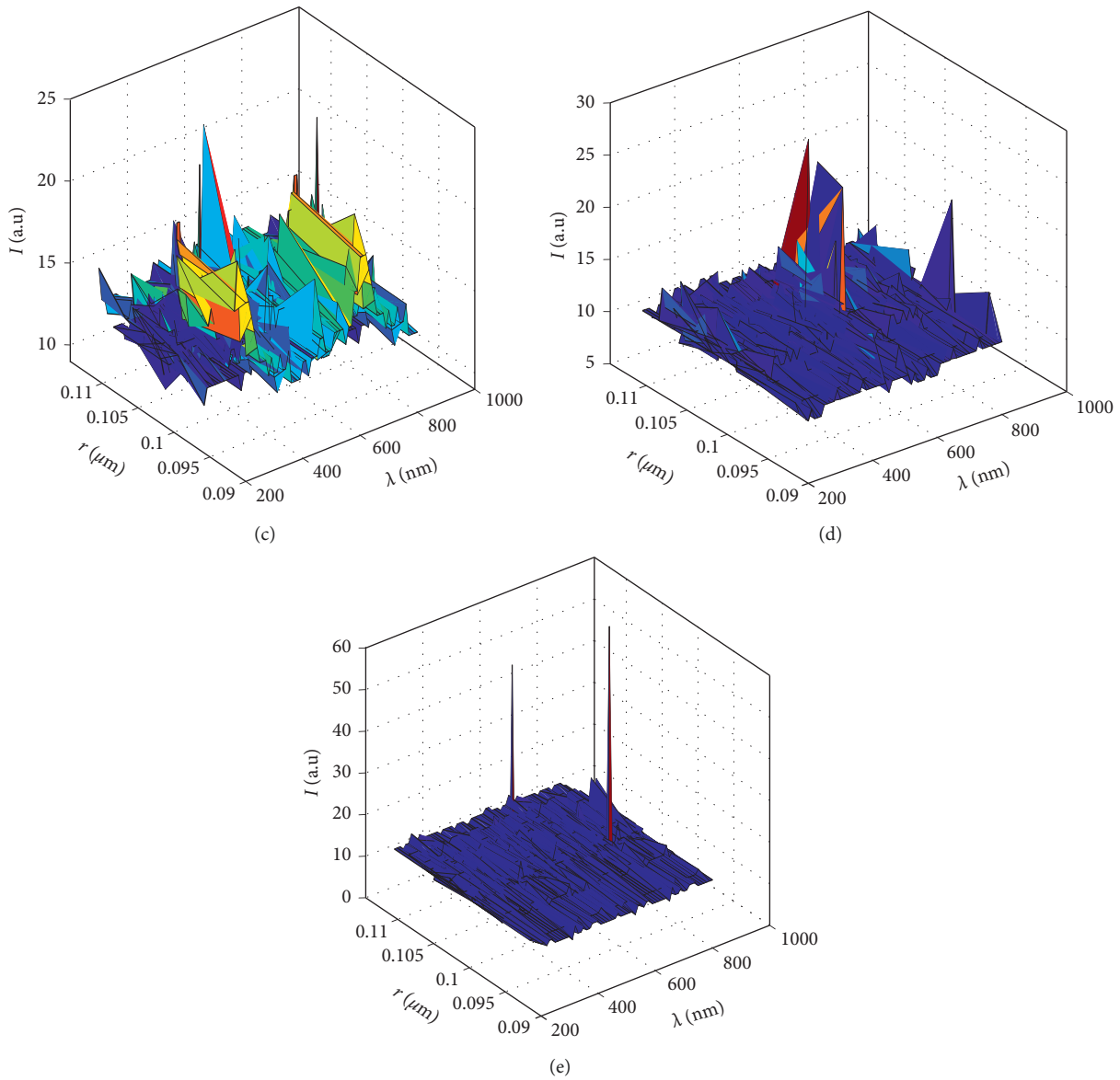

Figure 3: Three dimensional plots of pixel intensities/a.u (represented as I) and radii/μm (represented as r) against spectral range/nm (represented as λ) of multispectral images in the reflection mode for (a) uninfected RBCs (u-RBCs) and *Plasmodium falciparum*-infected RBCs (i-RBCs) of parasite density (PD) (b) (+), (c) (++), (d) (+++), and (e) (++++).

discriminants of u-RBCs and i-RBCs with PD (+, ++, +++, and ++++) in transmission mode for 435 nm illumination source. The data points for the u-RBCs and the i-RBCs are represented by (o) and (+), respectively. The star ($*$) in the middle is the classification midpoint between the u-RBCs and the i-RBCs. Figures 6(a)–6(d) show a clear linear discrimination of the u-RBCs and the i-RBCs from the midpoints, and the coefficient of PC1 is significant. This is as a result of PC1 retaining the most variations in the pixel intensities data. Figures 6(d) shows a data point of u-RBCs in the region of i-RBCs, and this could be an outlier. Other figures (not shown), for 660 nm in transmission mode and for 2-DSBs in reflection and scattering modes, exhibit similar linear discrimination pattern. Evaluation of the Fisher's linear discriminant function with the pixel intensities data shows total success of the discrimination function using the PCs of the u-RBCs and the i-RBCs in all the three modes. Figures 7–9(a) and 9(b) show a linear discrimination of the i-RBCs with different PD (+, ++, +++, and ++++) from the u-RBCs for the 2-DSBs. In reflection mode, Figures 7(a) and 7(b) and scattering mode, (Figures 8(a) and 8(b), a clear discrimination of the PD cannot be made easily for the 2-DSBs. Besides, the data points representing the PD for the 2-DSBs appear to be disrupted with low and/or similar pixel intensities. However, in transmission mode, Figures 9(a) and 9(b), the data points show a clear distinction of the PD for the 2-DSBs. The disparities in the discrimination may be due to the breakdown of Hb and increase rigidity in the i-RBCs by the parasite. For the

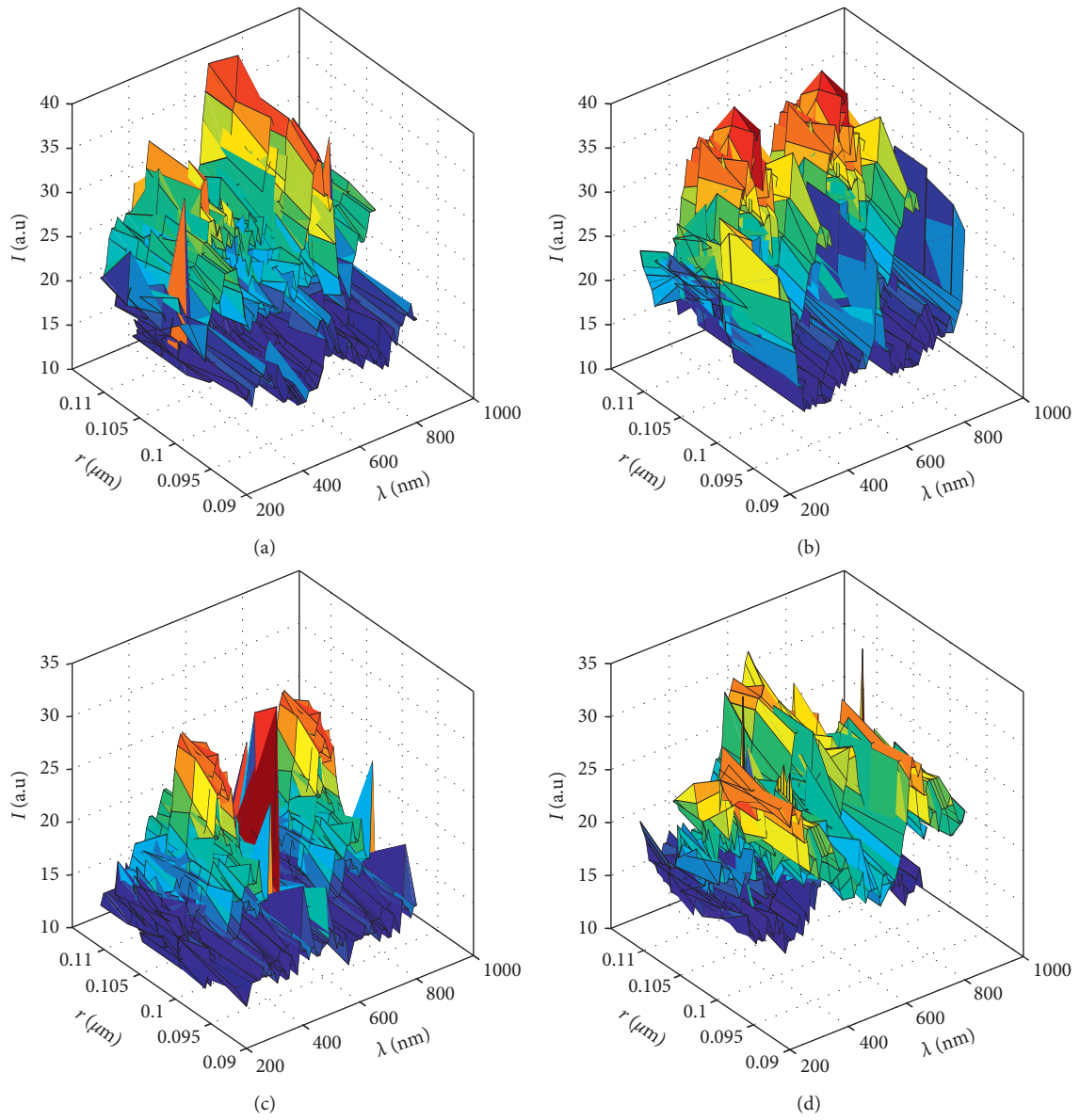

Figure 4: Continued.

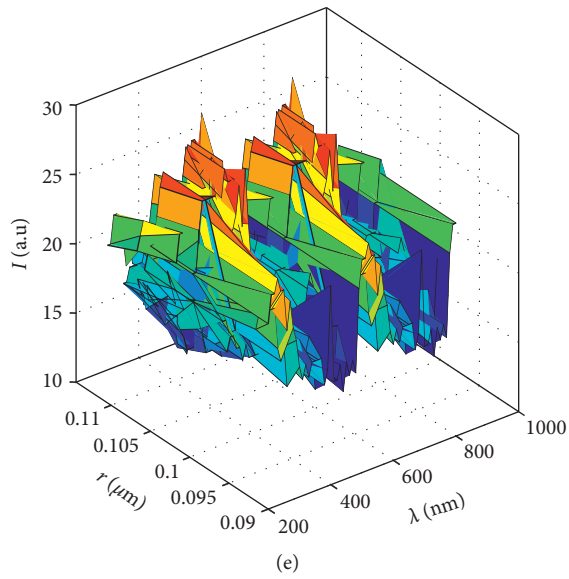

Figure 4: Three-dimensional plots of pixel intensities/a.u (represented as I) and radii/μm (represented as r) against spectral range/nm (represented as λ) of multispectral images in the scattering mode for (a) uninfected RBCs (u-RBCs) and *Plasmodium falciparum*-infected RBCs (i-RBCs) of parasite density (PD) (b) (+), (c) (++), (d) (+++), and (e) (++++).

various PD, increase in hemozoin accounts for low absorption and/or high transmission of incident light by the Hb, thereby increasing transmission and decreasing reflection and scattering of incident light. Hence, discrimination of i-RBCs with different PD could easily be done in transmission mode with illumination light sources of 435 nm and 660 nm.

4. Discussion

This work aims at the application of optical techniques to identify *P. falciparum* malarial byproduct (hemozoin) from human i-blood samples. The OA technique shows that the presence of *P. falciparum* parasites in the i-blood samples triggered Hb degradation with increasing PD and hence weak Hb absorption at the S-band (405 nm). At the β-band (541 nm), high ODs were observed for the u-blood samples and varied in the i-blood samples. These observations indicate that, at the β-band, there is high Hb absorption for all i-blood samples representing PD of (+) and weak Hb absorption for the samples with PD (++), (+++), and (++++), as a result of the growth of the parasite. And that, at the β-band, the PD estimation does not correlate either directly or inversely with Hb absorption.

Scatter plot of the ratio of β-band to α-band ODs as a product of the S-band ODs (Refer to Figure 1) shows that the presence of malaria parasites or increasing hemozoin in malarial patient's blood causes reduction in Hb degradation. When the constant factor k, which could be accounted for by the Drabkin's solution, is taken into consideration in the new (empirical) relation equation (3), say 0.04, the ratio of ODs for the u-blood samples approaches 1.00, suggesting that any value less than 1.00 is an infected blood with increasing PD. That for the i-blood samples show decrease ODs with increasing PDs. The value for i-blood samples are 0.69, 0.63, 0.42, and 0.30 for PD (+, ++, +++, and ++++), respectively. Compared with the u-blood samples, these values correspondingly decrease by 31.00%, 37.00%, 58.00%, and 70.00% for PD (+, ++, +++, and ++++).

The u-RBCs are cylindrically symmetric and are aligned parallel to an optical microscope slide containing blood smear. Therefore, optical orientation of u-RBCs and the i-RBCs onto a surface could reveal disparities in the RBCs as hemozoin shows bright white or cyan color in i-RBCs [24]. Exploiting the MSI technique, spectral differentiation could easily be made between the u-RBCs and the i-RBCs in all the three acquisition modes. The spectral differentiation between u-RBCs and i-RBCs was particularly observed by light intensity decrease in both reflection and scattering modes and increase in transmission mode for i-RBCs compared with u-RBCs, as shown in Figures 3–5. In transmission mode specifically, the spectra of Hb in u-RBCs were characterized by the S-band in the blue region and two additional bands in the green region [48]. The S-band uniquely depicted high absorption of Hb in u-RBCs (Figure 5(a)). This band tends to decrease and become broader in width with the presence of hemozoin (Figures 5(b)–5(e)), indicating low absorption and/or high transmission of light intensities by i-RBCs. This is an indication that the i-RBCs have their Hb either partially or completely digested together with the membrane proteins and membrane skeletal proteins by the parasite. The i-RBCs therefore become less dense and hence able to transmit more light [1, 2]. The intensity differences may be attributed to the breakdown of Hb by the parasite as protein chain fragments were transported away for further digestion. Also, the presence of hemozoin or the decrease of Hb could increase transmission of light. Therefore, incident radiation in the S-band was less absorbed by the i-RBCs. Hemozoin shows absorption bands at 630 and 660 nm in its fingerprints [36]. The 660 nm band was dominant in the spectral properties of

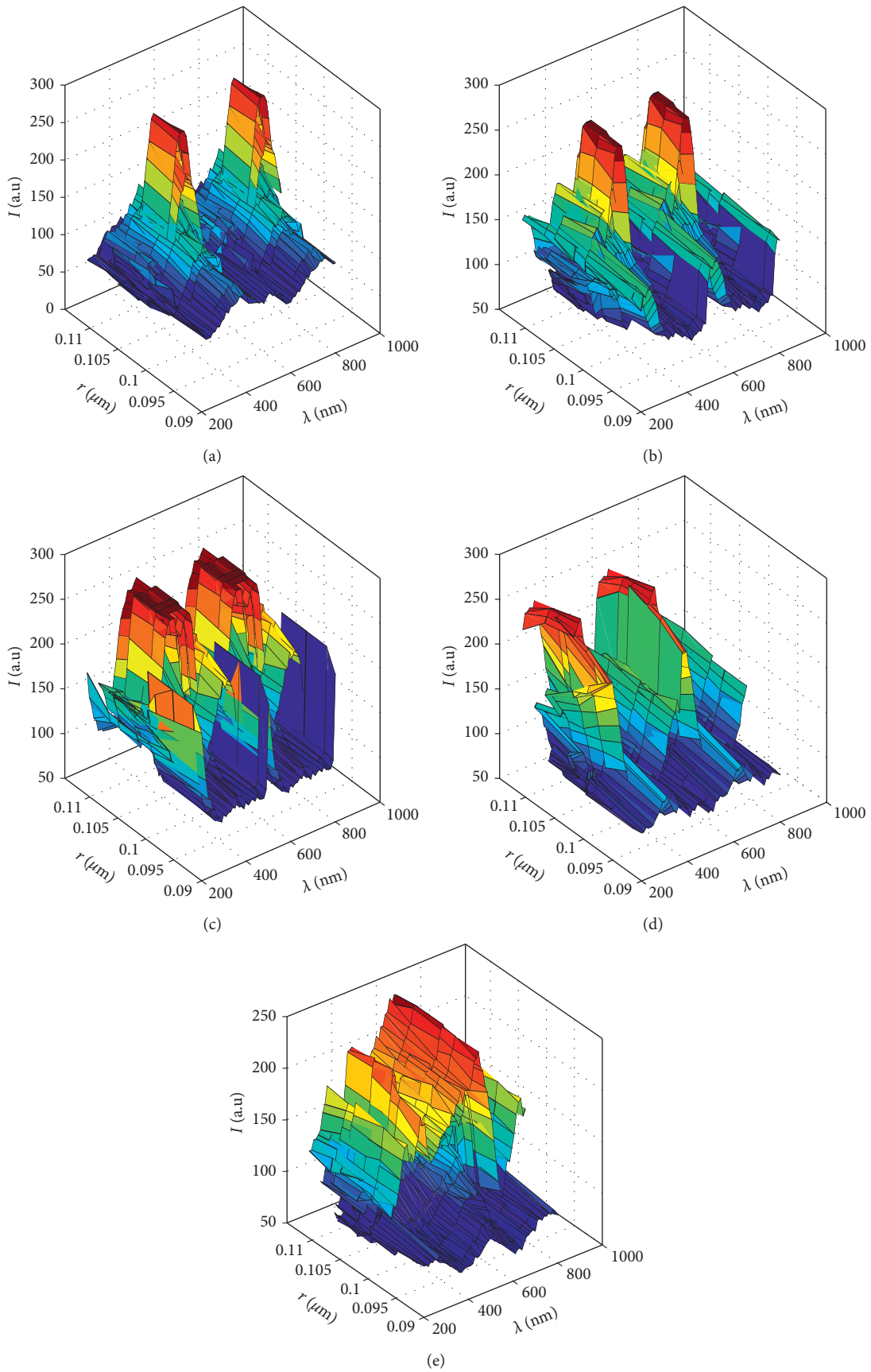

Figure 5: Three-dimensional plots of pixel intensities/a.u (represented as I) and radii/μm (represented as r) against spectral range/nm (represented as λ) of multispectral images in the transmission mode for (a) uninfected RBCs (u-RBCs) and *Plasmodium falciparum*-infected RBCs (i-RBCs) of parasite density (PD) (b) (+), (c) (++), (d) (+++), and (e) (++++).

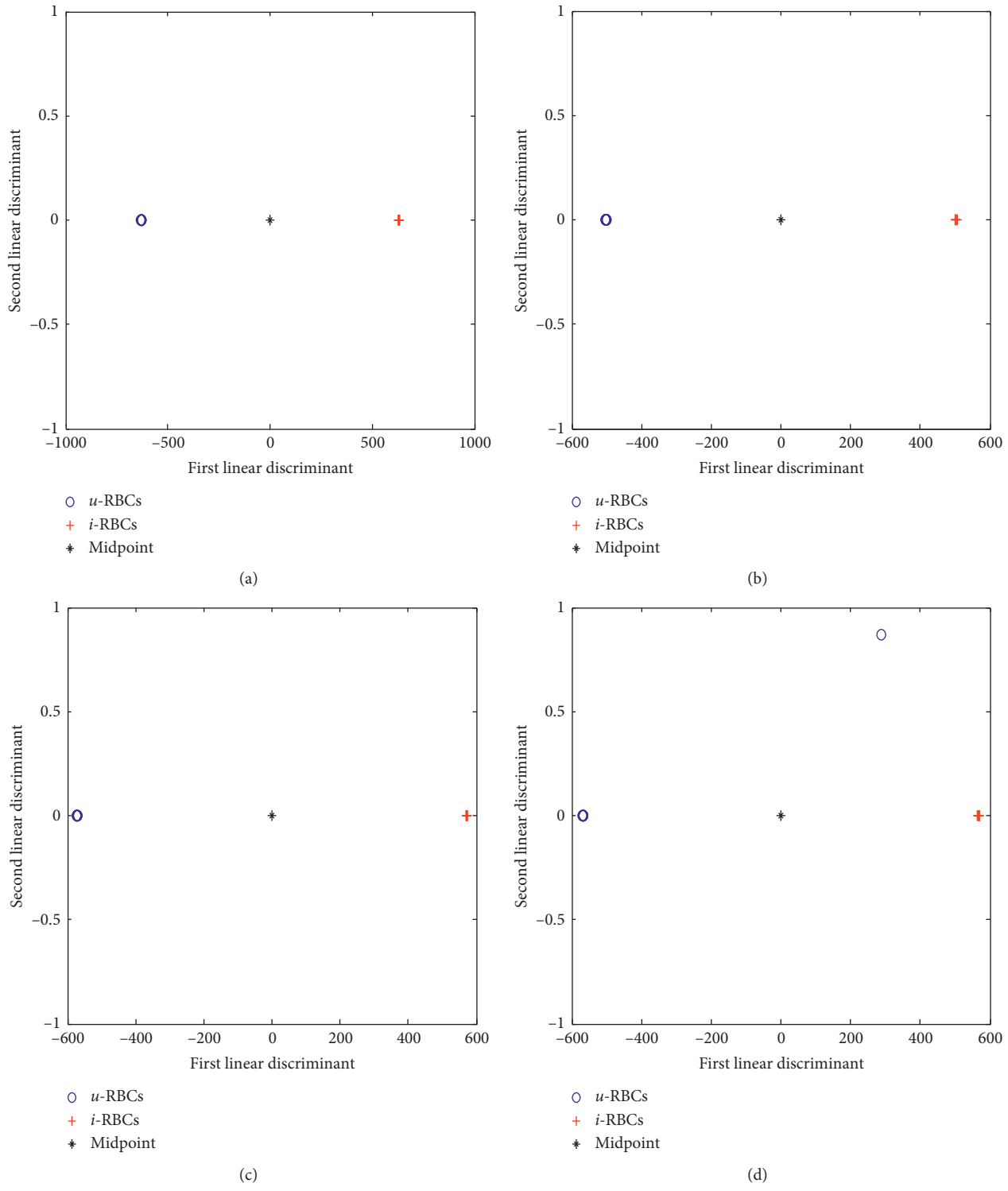

Figure 6: Scatter plots of first and second Fisher's linear discriminants showing transmitted pixel intensities of uninfected red blood cells (*u*-RBCs) and *Plasmodium falciparum*-infected human red blood cells *i*-RBCs (+) with parasite density: (a) (+), (b) (++), (c) (+++), and (d) (++++) for 435 nm illumination light source.

the *i*-RBCs in all three modes, especially in transmission mode. This shows that the 660 nm band could be identified to depict disparities between the *u*-RBCs and the *i*-RBCs in a blood smear slide under MSI microscope, which is in agreement with the work reported elsewhere [41]. Due to the biconcave shape of RBCs, the centers of the *u*-RBCs

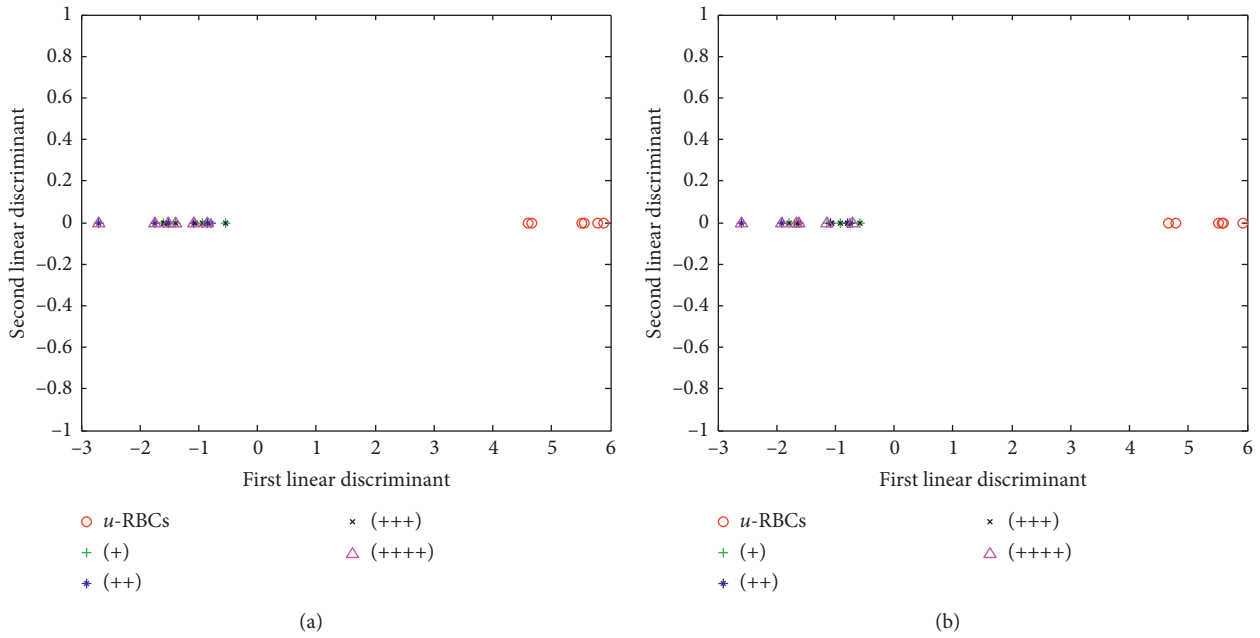

FIGURE 7: Scatter plots of first and second Fisher's linear discriminants showing reflected pixel intensities of uninfected red blood cells (*u*-RBCs) and *Plasmodium falciparum*-infected human red blood cells *i*-RBCs (+) with parasite density: (+), (++), (+++), and (++++) for (a) 435 nm and (b) 660 nm illumination light sources.

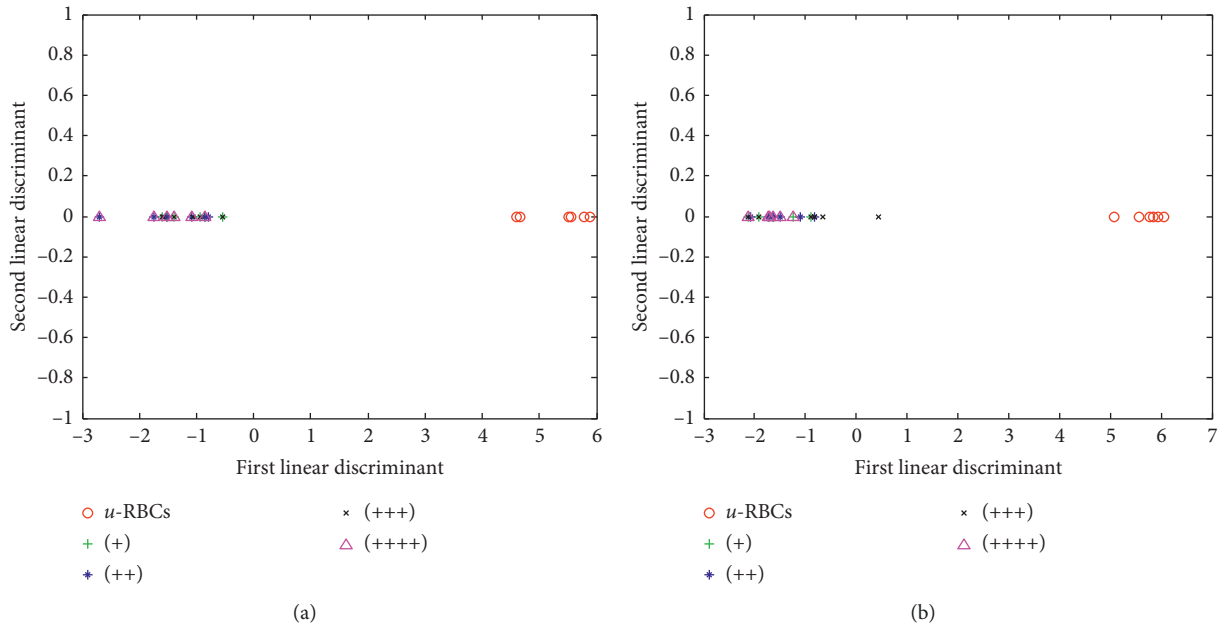

FIGURE 8: Scatter plots of first and second Fisher's linear discriminants showing scattered pixel intensities of uninfected red blood cells (*u*-RBCs) and *Plasmodium falciparum*-infected human red blood cells *i*-RBCs (+) with parasite density: (+), (++), (+++), and (++++) for (a) 435 nm and (b) 660 nm illumination light sources.

exhibited increase in reflected, scattered, and absorbed light intensities, whereas those of the *i*-RBCs depicted the inverse, suggesting symptoms of the level of infection, that is, the PD.

Fisher's linear discriminant analysis (FLDA) results (Figures 6–9) show midpoints for classifying the *i*-RBCs from the *u*-RBCs for the 2-DSBs as $(-6.7886, -2.8134, 5.8409$ and $8.9160) \times 10^{-15}$, $(55.2180, 5.7685, 1.2735$ and $-17.1130) \times 10^{-15}$, and $(787.7000, -1924.0000, 4801.1000$ and $4066.0000) \times 10^{-15}$ at 435 nm illumination light source congruently for PD (+, ++, +++, and ++++) in reflection scattering and transmission modes, respectively. The midpoints for 660 nm illumination light source in reflection, scattering, and transmission modes are, respectively, $(-12.6360, -32.4250, 13.0460$ and $13.3530) \times 10^{-15}$, (49.9240,

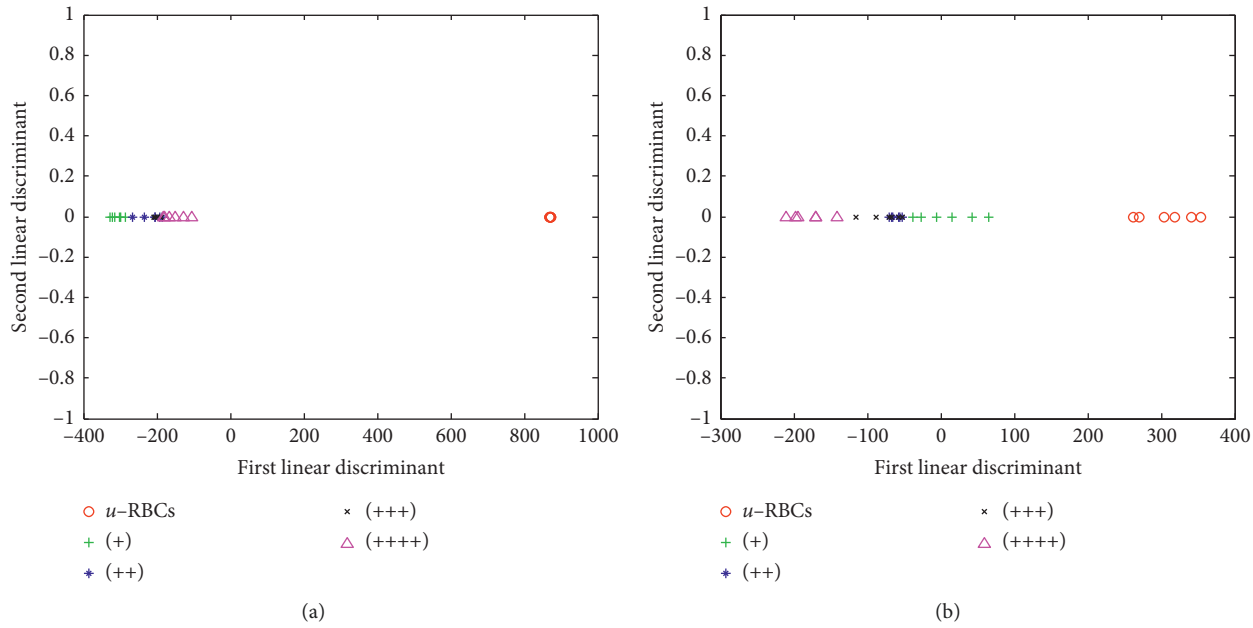

Figure 9: Scatter plots of first and second Fisher's linear discriminants showing transmitted pixel intensities of uninfected red blood cells (*u*-RBCs) and *Plasmodium falciparum*-infected human red blood cells *i*-RBCs (+) with parasite density: (+), (++), (+++), and (++++) for (a) 435 nm and (b) 660 nm illumination light sources.

-6.9688, 9.1570 and $49.9720) \times 10^{-15}$, and $(15.5970$, -36.2630, -484.0500 and $2.7970) \times 10^{-15}$ for PD (+, ++, +++, and ++++) correspondingly. It has been demonstrated that when using all three modes in the FLDA analysis, contrast could easily be made for the *u*-RBCs and the *i*-RBCs at the 2-DSBs with transmitted light.

5. Conclusion

This work shows the potential of two optical identification techniques, OA and MSI, based on fingerprints of blood absorption and spectral signatures of RBCs to estimate PD from *P. falciparum* human *i*-blood samples under staining-free preparations. Using the OA technique, empirical computation of the ratio ODs at blood absorption bands (*S*-band, β-band, and α-band) shows reduction in ODs with increasing PD in the *i*-blood samples. The OA technique exploited the disparities in the optical properties of the *i*-blood samples, indicating that *S*-band is an essential spectral band for Hb degradation, which could help to determine the severity of malaria.

By illuminating the blood samples with different LEDs in the three modes, we have shown the optical disparities between the *u*-RBCs and the *i*-RBCs with different PD without staining. Spectral differentiation between *u*-RBCs and *i*-RBCs is particularly observed by light intensity decrease in both reflected and scattered pixel intensities and increase in transmitted pixel intensities with increasing PD in *i*-RBCs. Blood, in general, shows strong absorption of visible light. Therefore, when the absorption property of blood is altered, such as the presence of malaria parasites in the *i*-RBCs, more light will be transmitted through the *i*-RBCs. Our work gives credence to the fact that Hb degradation in human blood increases with increasing PD in *i*-RBCs, and this is evidence in patients with severe malaria infections. Thus, the optical techniques applied in this work could offer potential tools for improved, point of care malaria diagnosis and therapy. Besides, we have proposed a linear classification model based on Fisher's approach [52] for the PD estimation.

Data Availability

The optical density and multispectral images data used to support the findings of this study are restricted by the Ghana Health Service Ethical Review Committee in order to protect volunteers privacy. Data are available from Dr. Jerry Opoku-Ansah upon request via e-mail: jopoku-ansah@ucc.edu.gh or mobile number +233 243333845 for researchers who meet the criteria for access to confidential data.

Conflicts of Interest

The authors declare that they have no conflicts of interest.

Acknowledgments

The authors express their heartfelt gratitude to International Programme for Physical Sciences (IPPS), International Sciences Programme (ISP), Uppsala University, Sweden, for providing travelling support to conferences, donation of microscopes, and other optical components. The authors also express their appreciation to the Office of External Activities and Associate scheme of Abdus Salam ICTP, Trieste, Italy, for funding and stay at ICTP. They thank all members of the African Spectral Imaging Network (AFSIN), Messrs. Jonathan Ntow and Emmanuel Birikorang of

Department of Laboratory Technology in the University of Cape for assisting in the OA measurements and statistical analysis, and finally, all members of Laser and Fibre Optics Centre (LAFOC) Research Group for their motivation and in-depth scientific contributions.

References

[1] D. E. Goldberg, A. F. Slater, R. Beavis, B. Chait, A. Cerami, and G. B. Henderson, "Hemoglobin degradation in the human malaria pathogen Plasmodium falciparum: a catabolic pathway initiated by a specific aspartic protease," *Journal of Experimental Medicine*, vol. 173, no. 4, pp. 961–969, 1991.

[2] L. R. Moore, H. Fujioka, P. S. Williams et al., "Hemoglobin degradation in malaria-infected erythrocytes determined from live cell magnetophoresis," *The FASEB Journal*, vol. 20, no. 6, pp. 747–749, 2006.

[3] S. E. Francis, D. J. Sullivan Jr., and D. E. Goldberg, "Hemoglobin metabolism in the malaria parasiteplasmodium falciparum," *Annual Review of Microbiology*, vol. 51, no. 1, pp. 97–123, 1997.

[4] R. Banerjee, J. Liu, W. Beatty, L. Pelosof, M. Klemba, and D. E. Goldberg, "Four plasmepsins are active in the Plasmodium falciparum food vacuole, including a protease with an active-site histidine," *Proceedings of the National Academy of Sciences*, vol. 99, no. 2, pp. 990–995, 2002.

[5] T. Frosch, S. Koncarevic, L. Zedler et al., "*In situ* Localization and structural analysis of the malaria pigment hemozoin," *The Journal of Physical Chemistry B*, vol. 111, no. 37, pp. 11047–11056, 2007.

[6] M. Loyevsky, T. LaVaute, C. R. Allerson et al., "An IRP-like protein from Plasmodium falciparum binds to a mammalian iron-responsive element," *Blood*, vol. 98, no. 8, pp. 2555–2562, 2001.

[7] J. A. Rowe, A. Claessens, R. A. Corrigan, and M. Arman, "Adhesion of Plasmodium falciparum-infected erythrocytes to humans cells: molecular mechanisms and therapeutic implications," *Expert Reviews in Molecular Medicine*, vol. 11, no. 16, pp. 1–29, 2009.

[8] P. Olliaro, "Editorial commentary: mortality associated with SeverePlasmodium falciparumMalaria increases with age," *Clinical Infectious Diseases*, vol. 47, no. 2, pp. 158–160, 2008.

[9] M. Hammer, D. Schweitzer, B. Michel, E. Thamm, and A. Kolb, "Single scattering by red blood cells," *Applied Optics*, vol. 37, no. 31, pp. 7410–7418, 1998.

[10] Y. Park, T. Yamauchi, W. Choi, R. Dasari, and M. S. Feld, "Spectroscopic phase microscopy for quantifying hemoglobin concentrations in intact red blood cells," *Optics Letters*, vol. 34, no. 23, pp. 3668–3670, 2009.

[11] A. Merdasa, "Multispectral microscopy with application to malaria detection," Master thesis, Division of Atomic Physics, Lund University, Lund, Sweden, 2010, https://lup.lub.lu.se/student-papers/search/publication/2260640/pdf.

[12] M. L. Dubey, C. Weingken, N. K. Ganguly, and R. C. Mahajan, "Comparative evaluation of methods of malaria parasite density determination in blood samples from patients and experimental animals," *Indian Journal of Medical Research*, vol. 109, pp. 20–27, 1999.

[13] A. Saussine, M.-A. Loriot, C. Picard et al., "Chloroquine cardiotoxicity in long term lupus therapy in two patients," *Annales de Dermatologie et de Vénéréologie*, vol. 136, no. 6-7, pp. 530–535, 2009.

[14] P. Murambiwa, B. Masola, T. Govender, S. Mukaratirwa, and C. T. Musabayane, "Anti-malarial drug formulations and novel delivery systems: a review," *Acta Tropica*, vol. 118, no. 2, pp. 71–79, 2011.

[15] M. D. Pammenter, "Techniques for the diagnosis of malaria," *South African Medical Journal*, vol. 74, no. 2, pp. 55–7, 1988.

[16] P. B. Bloland and M. Ettling, "Making malaria treatment policy in the face of drug resistance," *Annals of Tropical Medicine and Parasitology*, vol. 93, no. 1, pp. 5–23, 1999.

[17] C. Di Ruberto, A. Dempster, S. Khan, and B. Jarra, "Analysis of infected blood cell images using morphological operators," *Image and Vision Computing*, vol. 20, no. 2, pp. 133–146, 2002.

[18] N. E. Ross, C. J. Pritchard, D. M. Rubin, and A. G. Dusé, "Automated image processing method for the diagnosis and classification of malaria on thin blood smears," *Medical & Biological Engineering & Computing*, vol. 44, no. 5, pp. 427–436, 2006.

[19] D. Payne, "Use and limitations of light microscopy for diagnosing malaria at the primary health care level," *Bulletin of the World Health Organization*, vol. 66, no. 5, pp. 621–626, 1988.

[20] Oaks et al., "Malaria obstacles and opportunities," A Report of the Committee on the Study of Malaria Prevention and Control: Status Review and Alternative Strategies, National Academy Press, Washington, DC, USA, 1991.

[21] R. E. Coleman, K. Thimasarn, R. S. Miller et al., "Comparison of field and expert laboratory microscopy for active surveillance for asymptomatic Plasmodium falciparum and Plasmodium vivax in Western Thailand," *The American Journal of Tropical Medicine and Hygiene*, vol. 67, no. 2, pp. 141–144, 2002.

[22] K. Mitiku, G. Mengistu, and B. Gelaw, "The reliability of blood film examination for malaria at the peripheral health unit," *Ethiopian Journal of Health Development*, vol. 17, no. 3, pp. 197–204, 2003.

[23] I. Bates, V. Bekoe, and A. Asamoa-Adu, "Improving the accuracy of malaria-related laboratory tests in Ghana," *Malaria Journal*, vol. 3, no. 1, 2004.

[24] B. K. Wilson, M. R. Behrend, M. P. Horning, and M. C. Hegg, "Detection of malarial byproduct hemozoin utilizing its unique scattering properties," *Optics Express*, vol. 19, no. 13, pp. 12190–12196, 2011.

[25] W. G. Lee, Y.-G. Kim, B. G. Chung, U. Demirci, and A. Khademhosseini, "Nano/microfluids for diagnostic of infectious diseases in developing countries," *Advanced Drug Delivery Reviews*, vol. 62, no. 4-5, pp. 449–457, 2010.

[26] M. Brydegaard, A. Merdasa, H. Jayaweera, J. Ålebring, and S. Svanberg, "Versatile multispectral microscope based on light emitting diodes," *Review of Scientific Instruments*, vol. 82, no. 12, Article ID 123106, 2011.

[27] M. Saleem, M. Bilal, S. Anwar, A. Rehman, and M. Ahmed, "Optical diagnosis of dengue virus infection in human blood serum using Raman spectroscopy," *Laser Physics Letters*, vol. 10, no. 3, Article ID 035602, 2013.

[28] M. Bilal, M. Saleem, S. T. Amanat et al., "Optical diagnosis of malaria infection in human plasma using Raman spectroscopy," *Journal of Biomedical Optics*, vol. 20, no. 1, Article ID 017002, 2015.

[29] J. Michaelis, C. Hettich, J. Mlynek, and V. Sandoghdar, "Optical microscopy using a single-molecule light source," *Nature*, vol. 405, no. 6784, pp. 325–328, 2000.

[30] P. N. Prasad, *Introduction to Biophotonics*, Wiley-Interscience, Hoboken, NJ, USA, 2003.

[31] C. Yuen and Q. Liu, "Magnetic field enriched surface enhanced resonance Ramanspectroscopy for early malaria

diagnosis," *Journal of Biomedical Optics*, vol. 17, no. 1, Article ID 017005, 2012.

[32] Á. Orban, Á. Butykai, A. Molnár et al., "Evaluation of a novel magneto-optical method for the detection of malaria parasites," *PLoS One*, vol. 9, no. 5, Article ID e96981, 2014.

[33] J. L. Burnette, J. L. Carns, and R. Richards-Kortum, "Towards a needle-free diagnosis of malaria: in vivo identification and classification of red and white blood cells containing hemozoin," *Malaria Journal*, vol. 16, no. 1, p. 447, 2017.

[34] P. Teikari, *Multispectral Imaging. Course Project for AS-75.2128 Imaging and Displaytechnology*, Helsinki University of Technology, Espoo, Finland, 2008, http://www.petteriteikari.com/pdf/Teikari_Multispectral_Imaging.pdf.

[35] M. Brydegaard, Z. Guan, and S. Svanberg, "Broad-band multispectral microscope for imaging transmission spectroscopy employing an array of light-emitting diodes," *American Journal of Physics*, vol. 77, no. 2, pp. 104–110, 2009.

[36] Y. M. Serebrennikova, J. Patel, and L. H. Garcia-Rubio, "Interpretation of the ultraviolet-visible spectra of malaria parasite Plasmodium falciparum," *Applied Optics*, vol. 49, no. 2, pp. 180–188, 2010.

[37] Y. Park, M. Diez-Silva, D. Fu et al., "Static and dynamic light scattering of healthy and malaria-parasite invaded red blood cells," *Journal of Biomedical Optics*, vol. 15, no. 2, Article ID 020506, 2010.

[38] A. K. Dharmadhikari, H. Basu, J. A. Dharmadhikari, S. Sharma, and D. Mathur, "On the birefringence of healthy and malaria-infected red blood cells," *Journal of Biomedical Optics*, vol. 18, no. 12, Article ID 125001, 2013.

[39] D. M. Newman, J. Heptinstall, R. J. Matelon et al., "A magneto-optic route toward the in vivo diagnosis of malaria: preliminary results and preclinical trial data," *Biophysical Journal*, vol. 95, no. 2, pp. 994–1000, 2008.

[40] I. Silva, R. Lima, G. Minas, and S. O. Catarino, "Hemozoin and hemoglobin characterization by optical absorption towards a miniaturized spectrophotometric malaria diagnostic system," in *Proceedings of the 2017 IEEE 5th Portuguese Meeting on Bioengineering (ENBENG)*, February 2017.

[41] J. Opoku-Ansah, M. J. Eghan, B. Anderson, and J. N. Boampong, "Wavelength markers for malaria (Plasmodium falciparum) infected and uninfected red blood cells for ring and trophozoite stages," *Applied Physics Research*, vol. 6, no. 2, pp. 47–55, 2014.

[42] D. L. Omucheni, K. A. Kaduki, W. D. Bulimo, and H. K. Angeyo, "Application of principal component analysis to multispectral- multimodal optical image analysis for malaria diagnostics," *Malaria Journal*, vol. 13, no. 1, p. 485, 2014.

[43] A. Merdasa, M. Brydegaard, S. Svanberg, and J. T. Zoueu, "Staining-free malaria diagnostics by multispectral and multimodality light-emitting-diode microscopy," *Journal of Biomedical Optics*, vol. 18, no. 3, Article ID 036002, 2013.

[44] F. Kawamoto, "Rapid diagnosis of malaria by fluorescence microscopy with light microscope and interference filter," *The Lancet*, vol. 337, no. 8735, pp. 200–202, 1991.

[45] J. Opoku-Ansah, M. J. Eghan, B. Anderson, J. N. Boampong, and P. K. Buah-Bassuah, "Laser-induced autofluorescence technique for Plasmodium falciparum parasite density estimation," *Applied Physics Research*, vol. 8, no. 2, pp. 43–51, 2016.

[46] J. N. Boampong, E. O. Ameyaw, B. Aboagye et al., "The curative and prophylactic effects of xylopic acid onPlasmodium bergheiInfection in mice," *Journal of Parasitology Research*, vol. 2013, Article ID 356107, 7 pages, 2013.

[47] J. Opoku-Ansah, B. Anderson, M. J. Eghan, P. O.-W. Adueming, C. L. Y. Amuah, and S. S. Sackey, "A retrofitted metallurgical microscope using light emitting diodes for multi-spectral imaging," *Modern Applied Science*, vol. 11, no. 9, pp. 30–38, 2017.

[48] E. K. Hanson and J. Ballantyne, "A blue spectral shift of the hemoglobin soret band correlates with the age (time since deposition) of dried bloodstains," *PLoS One*, vol. 5, no. 9, Article ID e12830, 2010.

[49] E. Antonini and M. Brunori, "Hemoglobin and myoglobin in their reactions with ligands," in *Frontiers of Biology*, Vol. 21, North Holland Publishing Company, Amsterdam, Netherlands, 1971.

[50] F. Z. Okwonu and A. R. Othman, "A model classification technique for linear discriminant analysis for two groups," *International Journal of Computer Science Issues*, vol. 9, no. 3, pp. 125–128, 2012.

[51] P. O.-W. Adueming, M. J. Eghan, B. Anderson et al., "Multispectral imaging in combination with multivariate analysis discriminates selenite induced cataractous lenses from healthy lenses of sprague-dawley rats," *Open Journal of Biophysics*, vol. 7, no. 3, pp. 145–156, 2017.

[52] M. Welling, "Fisher linear discriminant analysis," Technical Report, University of Toronto, Toronto, Canada, 2000.